(Received 2 February 2026, Accepted 16 March 2026, Scheduled 15 April 2026)

Dual-Tuned Wideband Parasitically Loaded with Split-Ring Resonator Corner-Truncated Antenna for Sub-6 GHz Application

Atul Varshney[1, 2], Deepak Sharma[3], Jitendra Raghuwanshi[3], Rajesh Kumar Upadhyaya[4], Dunya Z. Mohammed[5], Abdul K. M. Zakir Hossain[6, *], and A. J. A. Al-Gburi[7, *]

[1]*ECE Department, FET, Gurukula Kangri (Deemed to be University), Haridwar, Uttarakhand 249404, India*
[2]*ECE Department, Graphic Era (Deemed to be University), Dehradun, Uttarakhand 248002, India*
[3]*ECE Department, Jaypee University of Engineering and Technology, Guna, Madhya Pradesh 473226, India*
[4]*Department of Electrical and Electronics Engineering, Mangalayatan University, Aligarh 202146, Uttar Pradesh, India*
[5]*Department of Electronic and Communications Engineering, Gilgamesh University, Baghdad 10001, Iraq*
[6]*Center for Telecommunication Research & Innovation (CeTRI)*
Fakulti Teknologi Dan Kejuruteraan Elektronik Dan Komputer (FTKEK)
Universiti Teknikal Malaysia Melaka (UTeM), Jalan Hang Tuah Jaya, Durian Tunggal, Melaka 76100, Malaysia
[7]*Strategic Research Institute (SRI), Asia Pacific University (APU)*
Jalan Teknologi 5, Taman Teknologi Malaysia, Kuala Lumpur 57000, Malaysia

ABSTRACT: A corner-truncated (linear and circular) antenna with a compressed reduced ground and parasitically loaded with a single unit of SRR was successfully designed, fabricated, tested, and investigated for 5G wireless communications. The truncated corner with a full ground shifted the narrow bandwidth and resonating frequency (5.10 GHz) from right to left (2.81 GHz). The ground-reduced length and compressed width enable a transition from a narrow band to a wide band, and the antenna is tuned to approximately 3.5 GHz. The antenna is parasitically loaded with an SRR that provides an additional resonating frequency within a wide bandwidth (2.82–5.21 GHz). The antenna achieves wideband with dual tuning frequencies within the band. The antenna has gains of 3.93 and 4.25 dBi at the tuned frequencies, respectively. The truncated ground enhances the antenna gain (3.33 to 4.25 dBi) and impedance bandwidth from narrow band (5.07–5.17 GHz) to wideband. The truncation of the corner and reduced ground length degrades the radiation efficiencies, while ground and substrate dimension (length and width) compression compensates for the reduced values of efficiencies. The proposed antenna is best suited for Wi-Fi 5 (IEEE 802.11ac), Wi-Fi 6 (IEEE 802.11ax), n48, n77, n78, and n79 applications. The antenna was measured and compared with the simulated results and radiation patterns. They were found in approximations, which helped confirm the antenna design and investigations.

1. INTRODUCTION

With the recent development of planar technology for 5G with a large number of closely spaced new radio (NR) Sub-6 GHz bands, a wideband antenna in the lower Sub-6 GHz frequency range (FR1) is highly desirable to cover important bands n77, n78, and n79. Therefore, a wideband antenna with a sufficient gain of approximately 4 to 5 dBi is required to solve this challenging issue. It is also desirable that the designed antenna be a wideband antenna to cover FR1 NR bands and Wi-Fi 5 for new-generation 5G and 6G applications. Different Wi-Fi and 5G FR1 new radio (NR) band standards are listed in Table 1.

Sharma et al. have designed a miniaturized ultra-wideband (UWB) circularly polarized antenna with enhanced axial ratio bandwidth, targeting C-band automotive and satellite applications, where the proposed structure demonstrates wide impedance bandwidth, stable circular polarization performance, and a compact form factor suitable for space-constrained wireless systems [1]. Varshney et al. have designed a transformer-fed monopole antenna for the n78 band. The corners of the square rhombus are truncated using a circular arc, which results in excellent miniaturization (85.33%), but the low gain (2.92 dBi) obtained is still an issue [2]. Varshney et al. created a 2×2 multiple-input multiple-output (MIMO) antenna using the circular truncation of a hexagonal patch with a parasitic stub loading for the 5G n78 band. It struggles to achieve a greater gain, even when employing a MIMO structure, but achieves an excellent size reduction of 86.74% for a single-element antenna [3]. A transformer-fed circular patch monopole antenna truncated with circular arcs was designed to cover the n78 band with 85.33% size miniaturization, and it attained a lower gain of 2.88 dBi [4]. In [5], a critical review was conducted to evaluate whether frequency-selective surfaces and metasurface reflectors are essential for antenna gain enhancement, highlighting scenarios where conventional metallic reflectors remain sufficient. Furthermore, a rectangular patch antenna with a parasitic SRR loaded in the ground

* Corresponding authors: Ahmed Jamal Abdullah Al-Gburi (ahmedjamal@ieee.org); Abdul Kayum Muhammad Zakir Hossain (zakir@utem.edu.my).

TABLE 1. 5G standards for Sub-6 GHz frequency range (FR1) new radio (NR) bands.

NR Standard	Frequency/Band (MHz)	NR Standard	Frequency/Band (MHz)	NR Standard	Frequency/Band (MHz)
Wi-Fi 5	5200	n7	2600	PCS	1900–1990
Wi-Fi 6E	5800	n40	2300	GSM	1800
n48	3550–3700	n41	2500	n2	1900
n77	3300–4200	n30	2300	n3	1800
n78	3300–3800	n34	2100	n25	1900
n79	4400–5000	n1	2100	n39	1900
n95	2100	n97	2300	n70	2000

and a U-stub in the patch is developed to cover all three 5G NR bands (n77, n78, and n79). However, it achieves a minimal overall decrease. The parasitically loaded SRR makes the antenna wideband dual-tuned at 3.24 GHz and 4.02 GHz. It also offers gain augmentation [6]. A UWB monopole antenna integrated with a mushroom-type electromagnetic band gap (EBG) structure is proposed to enhance bandwidth and gain, achieving a significantly wider impedance bandwidth (up to 23.33 GHz) and improved radiation performance compared to the conventional design, making it suitable for various wireless applications [7]. The SRR quadruplets are parasitically loaded onto an inset feed monopole compressed ground lotus-shaped antenna. The ground's shortened length and compressed width make the antenna wideband and allow it to be tuned at the designed frequency. The SRR-quadruplet parasitic loading in the ground increases the fractional bandwidth (FBW) from 39.07% (2.06–3.07 GHz) to 57.19% (1.61 GHz to 3.24 GHz). This antenna covers lower 5G NR bands n1, n7, n40, n41, n30, n34, n95, n97, without parasitic SRR quadruplet loading, and additionally covers with parasitic SRR quadruplet loading cellular PCS, GSM, 5G bands n2, n3, n25, n39, n70 [8]. This antenna fails to cover the n77, n78, and n79 bands. Therefore, an antenna is necessary that can cover all three 5G important NR bands within one wide band. Chidurala and Amara designed two antennas for 5G Sub-6 GHz applications to solve these existing issues. The first antenna is a slotted circular patch antenna parasitically loaded with a stub antenna, and the second is a 4-port fire-light-shaped MIMO antenna with a defected ground structure [9, 10]. A complementary split-ring resonator (CSRR) is loaded in the patch to eliminate the notch band and make the antenna wideband [11]. Mathew et al. have employed higher-order modes on a patch to generate tri-bands by designing a sector-shaped coaxial probe-fed three-corner truncated antenna. It covers only n78 of the Sub-6 GHz range and Wi-Fi 5 [12]. Bhattacharyya et al. have designed and fabricated a four-corner circular truncated, double-slotted antenna with reduced compressed ground for 5G NR (n77, n78) bands. It achieves 4.15 dBi of peak gain with a single unit and 6.15 dBi when arranged with a 4-element four-port MIMO configuration. An antenna achieved a tri-band reflection coefficient frequency response that covered the n77 and n78 bands along with WiFi 5 and WiFi 6E, but failed to achieve the n79 band [13]. Singh et al. constructed and measured a two-corner linearly truncated, multi-orbital elliptical slotted antenna for 5G high-speed wireless communication in the Sub-6 GHz band on a complete ground poly (dimethylsiloxane) (PDMS) substrate. It hits a peak gain of 3.0 dBi [14]. Banerjee et al. presented a comprehensive, technical review of circularly polarized antennas for different wireless applications [15]. Askari et al. have developed a coplanar waveguide (CPW)-fed circularly polarized wideband antenna for 5G Sub-6 GHz NR bands. It suffers from low gain, and it is enhanced by applying an artificial magnetic conductor (AMC) backed reflector [16]. Alsukour and Faouri have designed a side-edged, dual-band coaxial feed antenna for 5G and WiFi 6E [17]. Al Ka'bi published an article in which an antenna consisting of a full circle, semicircle, and meandered line was used for the Internet of Things (IoT) and WiFi 6 [18].

From the literature, it is clear that most studies either cover the NR n77/n78 bands or WiFi 5/WiFi 6. The designed antennas are either multiband with a lower gain value, or their structure consists of two linearly truncated opposite corners or two circularly truncated opposite corners. The wideband was achieved by either a reduced ground structure or a compressed width of the reduced ground. Consequently, it is highly recommended to use a high-gain antenna with four truncated corners that can cover all critical 5G NR bands (n77, n78, and n79) in conjunction with either high-speed WiFi 5 or WiFi 6, which has a wide bandwidth. Based on this research gap, in this study, a hybrid truncated-corner rectangular patch with the parasitic loading of SRR is presented to obtain the second tuning frequency, high gain, and wide bandwidth. Previous research also failed to achieve effective miniaturization to maintain gain and bandwidth. It has also been observed that as the antenna is loaded with a greater number of parasitic elements, the SRR increases the complexity of the structure, even though it helps to create more tuning frequencies within the band and enhances the gain of the antenna. The following are the primary objectives of this research:

- To design and develop a composite monopole microstrip antenna tailored for the 5G NR Sub-6 GHz frequency spectrum, specifically targeting the n77, n78, and n79 bands.

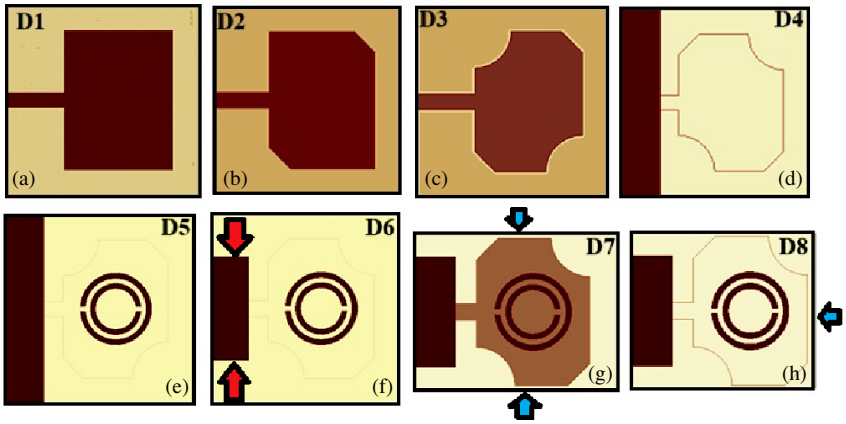

FIGURE 1. Step-by-step design development of a corner-truncated antenna structure.

- To investigate the influence of circular corner truncation and partial ground plane reduction on the impedance bandwidth and peak gain characteristics of the antenna.
- To examine the role of a parasitically loaded Split-Ring Resonator (SRR) in achieving dual-tuned reflection coefficient (S_{11}) responses and enhancing the overall selectivity of the operating bands.
- To optimize the antenna geometry to achieve a stable Axial Ratio (AR) and enhanced bandwidth, ensuring minimum signal reflection and robust polarization for high-fidelity 5G transmission and reception.

The novelty of this study is that a planar microstrip antenna is developed by truncating a rectangular patch antenna using an uncommon hybrid corner truncation (combination of linear and circular arcs). As we know, the gain and bandwidth product is always constant; therefore, with wider bandwidth, there will always be a chance of a decrease of antenna gain and radiation efficiency. The corner truncation reduces the copper in the patch, and therefore, along with reduced monopole ground, it also has additional advantage of lesser ohmic losses in the patch; hence, it results in improved efficiency along with adequate value of gain and bandwidth. Lesser bandwidth guarantees that there are always lower chances of in-band application interferences. The additional split ring resonator (SRR) in the ground results in an additional notch band within the wide bandwidth that isolates the n77, n78 bands with n79 and therefore reduces the application interferences. To reach the initial resonant frequency of 3.52 GHz for the n77 and n78 bands, the antenna ground was compressed along its width and length to achieve a wide bandwidth. Furthermore, the novel structure is loaded with a single unit of SRR in the ground to achieve an additional tuning frequency of 4.24 GHz in the n79 band within the same wide bandwidth as the original structure. This also prevents an increase in the fabrication complexity of antennas. Therefore, a hybrid corner-truncated microstrip wideband dual-tuned antenna is proposed for Sub-6 GHz 5G applications with an additional coverage of Wi-Fi 5. Miniaturized antennas with a substrate size of 30.55% were proposed, fabricated, and evaluated.

2. METHOD AND MATERIALS

The suggested 28 mm × 33 mm antenna for 3.40 GHz was fabricated on a low-profile FR4 substrate with a permittivity of 4.4, thickness of 1.6 mm, and loss tangent of 0.02.

2.1. Antenna Design Development and Geometry

The conventional design equations [19] are used for conventional microstrip rectangular patch antenna (RPA) [20–22] calculations. Initially, the dimensions of the conventional rectangular microstrip patch antenna (36.45 mm and 36.40 mm) were analysed at a design frequency of 3.40 GHz using conventional rectangular patch antenna design equations. It has a full bottom surface of an FR4 substrate ($\varepsilon_r = 4.4$, $\tan\delta = 0.02$) as ground, as shown in Figure 1(a). The corners of the rectangular patch are truncated using binary subtraction operations by considering four circles of radii 4.0 mm by selecting 4 line segments in two circles and 7.0 mm circles without selecting any line segments, as illustrated in Figures 1(b) and (c). Then, the ground length was reduced ($L_G = 7.2$ mm) toward the feed and compressed symmetrically 8.225 mm on each side around the feed concerning ground width in design 5 (D5), as displayed in Figures 1(e)–(f), and an SRR was attached to the bottom ground. In the next step, the substrate dimensions were compressed across the width and length. This determines the new dimensions of the miniaturized antenna, which is 28.0 mm × 33.0 mm, as displayed in Figures 1(g)–(h). Figures 2(a)–(c) show the optimized antenna construction, top view, rear view, and side view, and Table 2 lists all the corner-truncated antenna dimensions.

2.2. Design Development of Antenna

The comparisons of the reflection coefficients of the antenna design modification steps, as displayed in Figure 1, are shown in Table 3 and displayed in Figure 3(a). In design D1, a basic rectangular patch antenna with a full bottom ground surface establishes the fundamental and higher-order modes at ∼3.5 GHz and ∼5.1 GHz, and the reflection coefficient has a single narrow band and tuning frequency at 5.10 GHz with a peak gain of 3.33 dBi. In design D2, with two linear diagonal corner truncations perturbing the cavity to split the funda-

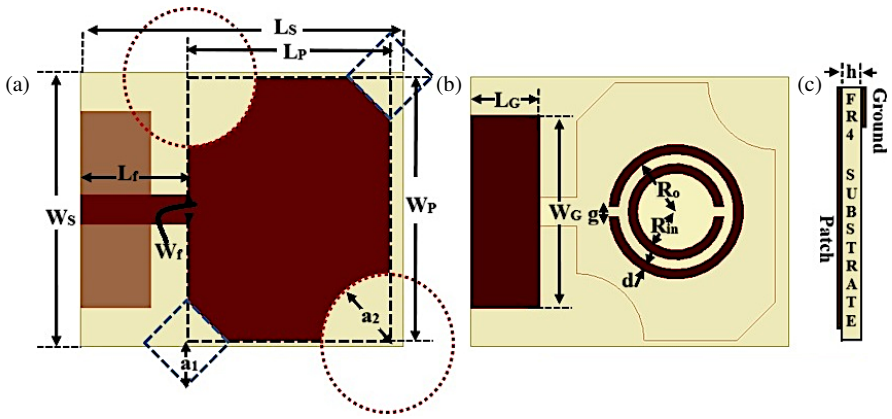

FIGURE 2. Proposed corner-truncated antenna geometry. (a) Front view, (b) rear view, and (c) side view.

TABLE 2. Dimensions of the proposed antenna.

Parameter Name	Parameter Designation	Dimensions (mm)
Substrate (FR4) $\varepsilon_r = 4.4$, $\tan\delta = 0.02$	Width: W_S	28.0
	Length: L_S	33.0
	Height: h	1.6
Ground (Copper)	Width: W_G	20.0
	Length: L_G	7.2
	Thickness: t	0.035
Patch (Copper)	Width: W_P	27.65
	Length: L_P	20.6
	Thickness: t	0.035
50 Ω Feed line	Feed width: W_f	3.0
	Feed length: L_f	11.0
First Circular Corner Cut	Radius: a_1 (line segments = 4)	3.0
Second Circular Corner Cut	Length: a_2 (line segments = 0)	7.0
Split Ring Resonator	Inner radius: R_{in}	4.0
	Outer radius: R_o	6.0
	Gap: g	1.0
	Width: d	1.0

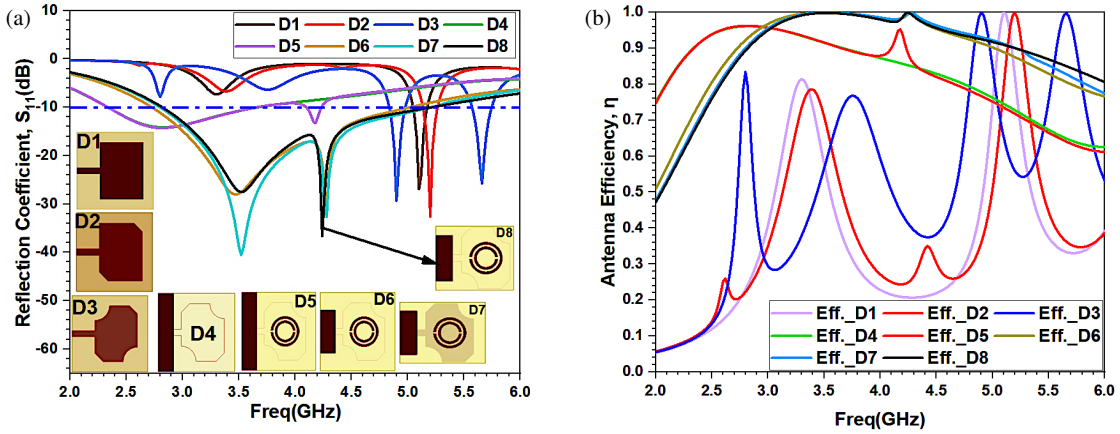

FIGURE 3. Compressions of corner-truncated patch antenna design development, (a) reflection coefficients and (b) radiation efficiencies.

mental modes into near-degenerate orthogonal modes, the reflection coefficients and gain improve because the linear corner truncation eliminates the accumulation of charges and helps to reduce reflections, whereas the tuning frequency shifts to 5.20 GHz. This truncation also shifts current paths diagonally, creating a nonuniform phase across the aperture. In design D3,

TABLE 3. Antenna design development.

Development Step	f_r (GHz)	$-S_{11}$ (dB)	-10 dB BW (GHz)	G (dBi) at f_r	η (%)
D1 with full ground	5.10	26.91	5.05–5.17	3.33	99.79
D2 with full ground	5.20	32.56	5.13–5.27	4.27	99.94
D3 with full ground	4.90 5.66	29.29 25.82	4.84–4.98 5.57–5.75	3.56 5.16	99.88 99.73
D4 with reduced ground	2.81	14.13	2.34–3.67	2.60	96.13
D5 with reduced ground + parasitic SRR loading	2.81 4.18	14.26 13.29	2.34–3.66 2.34–3.67	2.97 4.59	96.25 95.30
D6 with compressed reduced ground + parasitic SRR loading	3.48, 4.28	28.03, 30.73	2.73–5.02	3.74, 3.94	99.84 99.91
D7 with compressed substrate width	3.52, 4.28	40.55, 32.63	2.80–5.21	3.91, 4.28	99.99 99.94
D8 with compressed reduced ground + parasitic SRR loading	3.52, 4.24	27.52, 36.64	2.82–5.21	3.93, 4.25	99.82 99.97

* f_r: Tuning Frequency; S_{11}: Reflection Coefficient; BW: Bandwidth; G: Gain at f_r; η: Efficiency.

fine-tune the mode splitting to improve bandwidth and initiate circular polarization tendencies and also smoothen the current flow at the corners, reducing sharp-edge parasitic reflections. With four truncated opposite (linear and circular) corners, the reflection coefficient plot becomes dual bands, and the gain improves at the upper tuning frequency 5.66 GHz while decreasing at the lower tuning frequency 4.90 GHz. In design D4 with reduced ground, transform the antenna from a narrowband cavity to a wider-band monopole-like radiator. The fringing fields significantly increase at the patch-ground gap, broadening the impedance bandwidth. The reflection coefficient decreases; the -10 dB bandwidth becomes wider from 2.34 GHz to 3.67 GHz; and the tuning frequency shifts to 2.81 GHz. In design D5, the integration of an SRR in the ground introduces a sub-wavelength magnetic resonance that couples with the patch modes. It creates a secondary "hot spot" of current in the ground plane, shifting the lower frequency resonance. This parasitic loading of the ground with an SRR introduces a new resonating frequency at 4.18 GHz, and the reflection coefficient becomes dual-band in nature. The reduced value of gain in the previous stage is slightly improved in this stage due to the introduction of SRR loading. In design D6, the ground width is reduced (ground plane width tuning), which optimizes the coupling between the partial ground and the feed line and results in a dip at the center frequency. This also compresses the ground width, making the antenna reflection coefficient frequency response wideband (2.73 GHz to 5.02 GHz), dual-tuned (3.48 GHz and 4.28 GHz). This ground compression also adjusts the characteristic impedance of the input, smoothing the aperture power flow, which improves the reflection coefficient and lower frequency 3.48 GHz gain in comparison to the previous step. In design D7, substrate width compression adjusts the effective permittivity to pull the higher-order modes closer to the fundamental. Concentrate the E-field within the dielectric, narrowing the aperture beamwidth for higher gain. The substrate width decreases to 28 mm, which will further improve the reflection coefficients at the two resonating frequencies and widen the bandwidth with the improvement in gain at the two frequencies. In design D8, the substrate length is compressed (with a reduced substrate length of 33 mm), which aligns all resonant peaks (3.5 and 4.2 GHz) into a single wideband response and achieves a balanced current distribution across the patch and SRR, ensuring wideband matching. The reflection coefficient value degrades this miniaturized proposed antenna at lower resonating frequency, and gain improves while at upper frequencies, it also increases, and at upper resonating frequency, the reflection coefficient value increases. The radiation efficiencies in the Sub-6 GHz of the corner-truncated reduced ground antenna were investigated and compared in Figure 3(b). It has been noticed that the antenna bandwidth becomes widened while the radiation efficiency degrades from 99% to 96% with reduced ground length. The parasitic loading further reduces the efficiency to 95%. This decreased value of radiation efficiency is further increased to 99% by compressing the ground width, and the further improvement in the radiation efficiency is investigated with compression of the substrate width and its reduced length.

2.2.1. Modal Analysis and Corner Truncation

Based on the "step-by-step design development", the generation of orthogonal modes is a systematic process of introducing physical dimensions of the antenna structure to a symmetric structure. This section explains how the orthogonal modes are generated and accessed through the design modifications.

1. The Initial State (D1): Fundamental Modes

In stage D1, the antenna is a standard rectangular patch. The electromagnetic fields are analyzed as Transverse Magnetic (TM) modes because the thickness of the substrate (h) is much smaller than the wavelength, causing the electric field to be nearly perpendicular to the patch. There are two primary

transverse magnetic (TM_{mn}) modes, where m and n represent the number of half-wave field variations along the length (L_P) and width (W_P) of the patch.

The TM_{10} mode is the most commonly used fundamental mode of radiation: The current flows along the length (L_P) of the patch, and in TM_{01} mode, the current flows along the width (W_P) of the patch. Because the structure is rectangular and fed by a single microstrip line, these modes are typically excited independently or remain "degenerate" (overlapping), resulting in linear polarization. The resonant frequency (f_{mn}) for the TM_{mn} mode is given by:

$$f_{mn} = \frac{c}{2\sqrt{\varepsilon_{eff}}}\sqrt{\left(\frac{m}{L_{eff}}\right)^2 + \left(\frac{n}{W_{eff}}\right)^2} \quad (1)$$

where for a microstrip patch, $W_P/h > 1$ $(27.65/1.6 \approx 17.2)$

$$\varepsilon_{eff} = \frac{\varepsilon_r + 1}{2} + \frac{\varepsilon_r - 1}{2}\left(1 + \frac{12h}{W_P}\right)^{-\frac{1}{2}} \quad (2)$$

For an FR4 substrate of thickness $h = 1.6$ mm, the estimated ε_{eff} is 4.09.

The length $L_P = 20.6$ mm determines the primary resonance. The extension length ΔL due to fringing fields was estimated to be 0.75 mm.

$L_{eff} = L_P + 2\Delta L = 20.6 + 1.5 = 22.1$ mm and $W_{eff} = W_P + 2\Delta L = 27.65 + 2(0.75) = 29.15$ mm.

$$f_{10} = \frac{3\times10^8}{2\sqrt{4.09}}\sqrt{\left(\frac{1}{22.1}\right)^2 + \left(\frac{0}{29.15}\right)^2} \approx 3.36\,\text{GHz}$$

This mode corresponds to the primary 5G resonance seen in the S_{11} results.

2. Perturbation through Truncation (D2 & D3)

The critical step for orthogonal mode generation occurs in stages D2 and D3:

Corner Truncation: By removing the corners of the patch (first circular-cut $a1 = 3.0$ mm and second circular-cut $a2 = 7.0$ mm), the symmetry of the patch is disturbed.

Mode Splitting: This physical perturbation causes a single resonance to split into two near-degenerate orthogonal modes.

Phase Quadrature: The truncations are sized specifically to ensure that one mode is slightly delayed relative to the other. When these two orthogonal modes are excited with equal magnitudes and a 90° phase difference, circular polarization (CP) is achieved. The width $W_P = 27.65$ mm was used to calculate the orthogonal mode (TM_{01}) resonance.

$$f_{01} = \frac{3\times10^8}{2\sqrt{4.09}}\sqrt{\left(\frac{0}{22.1}\right)^2 + \left(\frac{1}{29.15}\right)^2} \approx 2.55\,\text{GHz}$$

In the design evolution, the corner truncations (D2, D3) and the feed line $W_f = 3.0$ mm act to "pull" this resonance higher toward the TM_{10} mode to create a circular polarization region.

3. Structural Refinement (D4–D6)

In these modification stages, the ground plane and feed transition are modified:

Partial Ground Plane: Moving from a full ground to a partial ground ($L_G = 7.2$ mm) modifies the fringing fields, which helps broaden the impedance bandwidth of the generated modes.

Resonator Integration: The addition of the SRR in D5 and D6 introduces additional resonant paths. This further manipulates the field distribution, allowing the orthogonal modes to maintain their relationship across a wider frequency range, as observed in the broadened S_{11} curve for D6.

4. Final Optimization (D7 & D8)

The final stages focus on balancing the modes: The final tweaks to the patch boundary (indicated by the blue and red arrows in D7/D8) serve to fine-tune the coupling between orthogonal modes.

The result is a stable, wide-band resonance centered near 3.5 GHz, and a secondary resonance at 4.25 GHz, where the orthogonal components are optimally combined for performance. This hybrid mode (TM_{11}) arises from the diagonal-field distribution across the patch.

$$f_{11} = \frac{3\times10^8}{2\sqrt{4.09}}\sqrt{\left(\frac{1}{22.1}\right)^2 + \left(\frac{1}{29.15}\right)^2} \approx 4.25\,\text{GHz}$$

This perfectly matched the second major resonance dip observed in the S_{11} curve (D8) at approximately 4.25 GHz.

2.3. Effect of Parasitic SRR Loading on Proposed Antenna

Resonator integration of the SRR in design D5 introduces additional resonant paths. It further modifies the field distribution, allowing the orthogonal modes to maintain their relationship across a wider frequency range, as observed in the broadened S_{11} curve for D6. The designed SRR with its boundary conditions is illustrated in Figure 4(a). It is clearly observed from its reflection coefficient magnitude and phase plot that the lowest S_{11} magnitude is obtained near 4.27 GHz with a phase change from $-180°$ to $180°$. It shows a resonating frequency at 4.27 GHz.

The reflection coefficient of the parasitic SRR-loaded truncated proposed antenna in design D8 is compared with that of the truncated corner antenna without SRR-loading in Figure 4(b) and is shown in Table 4. The graphs show that without parasitic SRR loading, the antenna has a single-tuned wide bandwidth from 2.79 to 30 GHz, with a gain of 3.70 dBi at 3.54 GHz. However, parasitic loading of this antenna with the SRR adds a 4.24 GHz resonating frequency and improves the gains at two frequencies and the antenna reflection coefficient frequency response.

The SRR reflection coefficient magnitude and phase are illustrated in Figure 4(a), which indicates the lowest reflection coefficient value at 4.27 GHz and a change in phase from $-180°$ to $180°$. It is shown that the addition of SRR in the patch antenna plays an important role, resulting in an additional resonating frequency near 4.27 GHz along with 3.5 GHz resonance. Therefore, the frequency response of the antenna becomes dual-tuned.

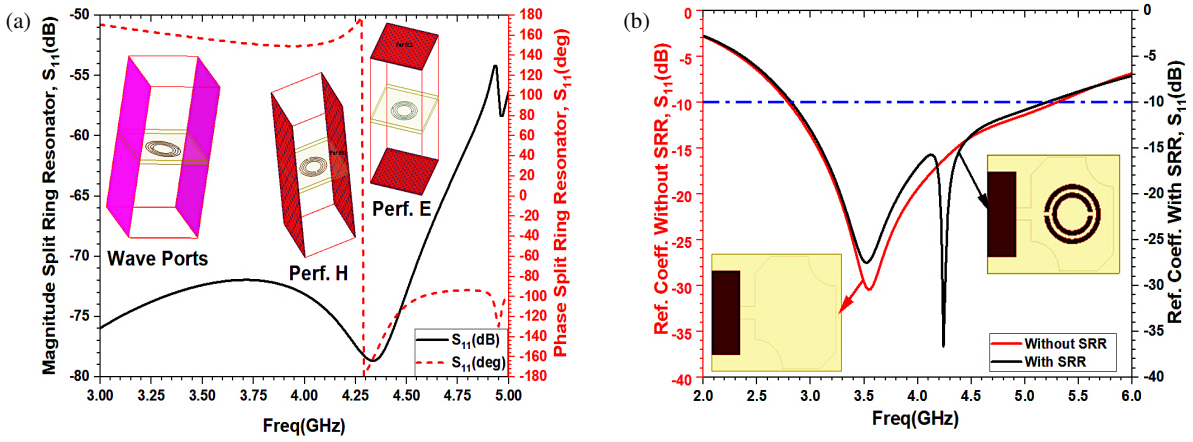

FIGURE 4. Influence of SRR loading. (a) Magnitude and phase of SRR. (b) S_{11} of parasitic SRR loading on patch antenna.

TABLE 4. Parasitic SRR loading of antenna.

SRR Loading	f_r (GHz)	$-S_{11}$ (dB)	-10 dB BW (GHz)	G (dBi) at f_r
D8 compressed reduced ground without SRR	3.54	30.45	2.79–5.30	3.70
D8 with compressed reduced ground + parasitic SRR loading	3.52, 4.24	27.52, 36.64	2.82–5.21	3.93, 4.25

* f_r: Tuning Frequency; S_{11}: Reflection Coefficient; BW: Bandwidth; G: Gain at f_r; η: Efficiency.

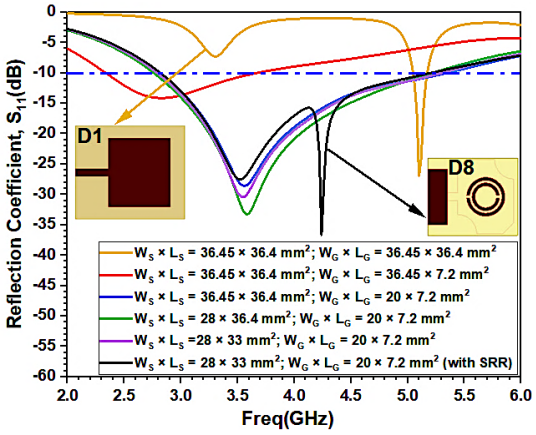

FIGURE 5. Reflection coefficients of antenna miniaturization.

2.4. Effect of Compressed Reduced Ground Length and Antenna Miniaturization

As indicated in step 1 (D1) of Figure 1, a rectangular patch antenna was developed with a full ground plane of length and widths equal to the substrate. This results in a very narrow bandwidth with a -26.91 dB reflection coefficient. As illustrated in step 4 (D4) of Figure 1, the ground length was shortened towards the feed end to 7.2 mm from the rectangular patch to improve bandwidth. Increased gain and -10 dB FBW were achieved, with a resonance frequency shift from 5.10 to 2.81 GHz. To further improve the bandwidth, the reduced ground was compressed symmetrically in width from its center by 8.225 mm in design D4. It increases the -10 dB FBW from 2.82 to 5.35 GHz and enhances the gain at 3.56 GHz. In all three stages, no change in the substrate width and length was carried out, i.e., 0% miniaturization in size. Now the width of the substrate is reduced, which improves the reflection coefficient to -33.27 dB. The antenna was 23.18% smaller after this adjustment. The antenna substrate length was reduced to 33 GHz. This reduces the antenna gain while widening the antenna bandwidth, resulting in 30.55% antenna size miniaturization and tuning the antenna to 3.54 GHz. Finally, the antenna ground was parasitically loaded with an SRR, which not only improved the gain but also introduced a second tuning frequency at 4.24 GHz along with a lower tuning frequency at 3.52 GHz. Figure 5 compares the reflection coefficient (S_{11}) plots of the reduced, compressed, and full ground, and Table 5 lists their parameter information.

2.5. Effect of Corner Truncated Patch

Consideration of corner truncation: It is noticed that the excessive charges accumulate across corners of the rectangular patch antenna. Therefore, to remedy this issue, corner truncation is considered in the proposed work. This truncation minimizes the charge accumulation and thereby the reflections. This will improve the reflection coefficient value.

The antenna patch was initially designed to be rectangular. No corners were cut. A peak gain of 4.21 dBi was achieved at 3.64 GHz with a bandwidth of 2.92–4.65 GHz. The linear truncated opposite corners reduce the gain by 4.02 dBi but increase the bandwidth (2.90–4.79 GHz). Furthermore, the additional circular truncated corners introduce an additional tuning frequency at 4.24 GHz and shift the lower resonating frequency to 3.52 GHz. This also significantly improved the reflection

TABLE 5. Antenna miniaturization.

Change in Ground Size of Rectangular Patch	f_r (GHz)	$-S_{11}$ (dB)	-10 dB BW (GHz)	G (dBi) at f_r	Mini. (%)
With full ground (D1), $W_G \times L_G = 36.45 \times 36.4\,\text{mm}^2$ $(W_S \times L_S = 36.45 \times 36.4\,\text{mm}^2)$	5.10	26.91	5.05–5.17	3.33	0
With reduced ground length (D4), $W_G \times L_G = 36.45 \times 7.2\,\text{mm}^2$ $(W_S \times L_S = 36.45 \times 36.4\,\text{mm}^2)$	2.81	14.13	2.34–3.67	2.60	0
D4 With Compressed Ground Width $W_G \times L_G = 20 \times 7.2\,\text{mm}^2$ $(W_S \times L_S = 36.45 \times 36.4\,\text{mm}^2)$	3.56	28.61	2.82–5.35	3.82	0
With compressed Substrate width without SRR (D7) $W_G \times L_G = 36.45 \times 7.2\,\text{mm}^2$ $(W_S \times L_S = 28 \times 36.4\,\text{mm}^2)$	3.58	33.27	2.76–5.22	3.99	23.18
With compressed Substrate width and length without SRR (D7) $W_G \times L_G = 36.45 \times 7.2\,\text{mm}^2$ $(W_S \times L_S = 28 \times 33\,\text{mm}^2)$	3.54	30.45	2.79–5.30	3.70	30.35
With compressed reduced ground with SRR (D8) $W_G \times L_G = 36.45 \times 7.2\,\text{mm}^2$ $(W_S \times L_S = 28 \times 33\,\text{mm}^2)$	3.52, 4.24	27.52, 36.64	2.82–5.21	3.93, 4.25	30.35

* f_r: Tuning Frequency; S_{11}: Reflection Coefficient; BW: Bandwidth; G: Gain at f_r; η: Efficiency; Min.: Miniaturization.

TABLE 6. Effect of corner truncation of rectangular patch.

Corner Truncation	f_r (GHz)	$-S_{11}$ (dB)	-10 dB BW (GHz)	G (dBi) at f_r
No	3.64	16.88	2.92–4.65	4.21
With linear truncated two-corners	3.64	19.32	2.90–4.79	4.02
With linear plus circular truncated four-corners	3.52, 4.24	27.52, 36.64	2.82–5.21	3.93, 4.25

* f_r: Tuning Frequency; S_{11}: Reflection Coefficient; BW: Bandwidth; G: Gain at f_r; η: Efficiency.

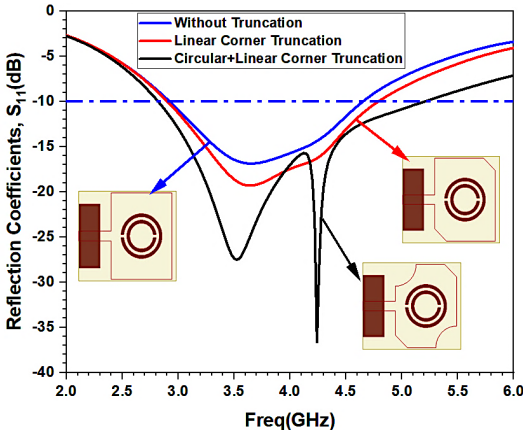

FIGURE 6. Effect of truncated corner patch.

coefficient at both resonating frequencies. The reflection coefficient (S_{11}) plots are shown in Figure 6, and the resultant parameter values are listed in Table 6.

2.6. Fabricated Antenna

The antenna was fabricated on a 28 mm × 33 mm FR4 substrate using artwork, UV exposure, and chemical etching. Next, a 50 Ω SMA connector was carefully soldered near the feed width center of the antenna. Figures 7(a)–(b) show the front and rear views of the antenna prototype with dimensional measurements.

3. RESULTS AND DISCUSSIONS

3.1. Antenna Reflection Coefficient

The reflection coefficient of the designed antenna was computed using High Frequency Structure Simulator (HFSS) software and compared with the reflection coefficient measured using a vector network analyzer (Agilent Technologies N5247A). The simulated and measured reflection coefficient curves of the proposed parasitically SRR-loaded flag-shaped antenna are shown in Figure 8. The simulations show resonance frequencies of 3.52 and 4.24 GHz (HFSS), whereas the measured frequencies are 3.31 and 4.26 GHz. The 10 dB fractional bandwidth (FBW) in the simulated plot is 67.89% (2.82 GHz–5.21 GHz), while in the measured plot, this value is 88.52% (2.52 GHz–5.58 GHz). A 0.21 GHz shift was observed in the lowest-resonating frequency. This minor difference in the measured value might be due to the material selection and its different physical properties in the loss tangent, improper soldering,

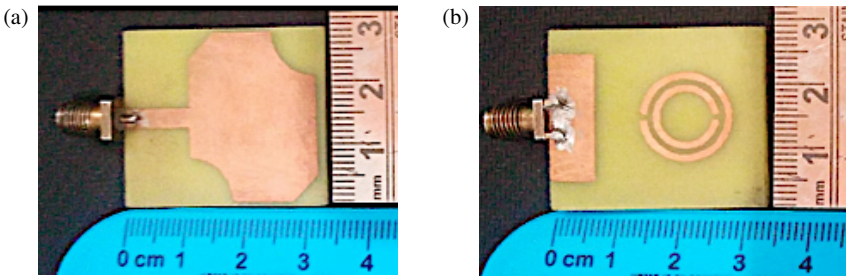

FIGURE 7. Fabricated antenna, (a) front view, (b) rear view.

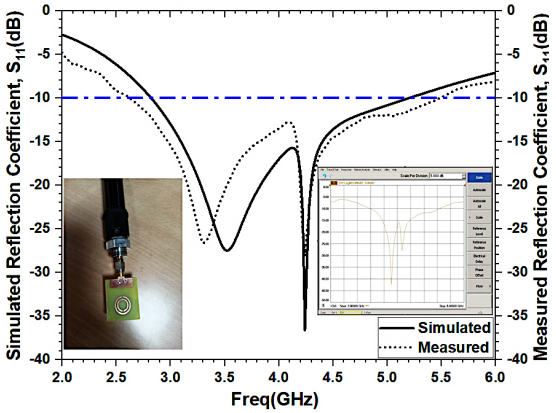

FIGURE 8. Reflection coefficients plots.

or soldering loss. Thus, the measured and simulated reflection coefficients were in good agreement.

3.2. Antenna Radiation Patterns

Figures 9(a)–(d) show the simulated and measured E- and H-plane gain radiation patterns of the antenna at resonance frequencies of 3.52 and 4.24 GHz, respectively. The antenna exhibited good omnidirectional radiation patterns in the E- and H-planes at the two resonating frequencies. Both planes exhibited similar gain radiation patterns in the simulation and measurements. The simulated and measured results concurred, indicating that the antenna was well modelled and fabricated. However, slight variations between the simulated and measured findings demonstrate the significance of thorough measurements and simulations to maintain accuracy. These disparities may have been caused by measurement errors, fabrication tolerances, or simulation flaws. The half-power beamwidth (HPBW) values help determine the antenna coverage, gain, and directivity. The directional properties of the antenna are shown by the half-power beamwidth (HPBW) and front-to-back ratio (FBR).

3.2.1. Radiation Patterns at 3.52 GHz

E-Plane Pattern: The radiation pattern was approximately circular, indicating that the antenna had a relatively omnidirectional radiation pattern in the E plane. The pattern showed slight asymmetry, with a deeper null at approximately 270° than at 90°. The gain was approximately 2 dB at 0° (or 360°) in the direction of maximum radiation. From Figure 9(a), the front-to-back ratio (FBR) is estimated to be approximately 10 dB.

H-Plane Pattern: In contrast, the H-plane pattern at 3.52 GHz [Figure 9(b)] displays a more directional radiation pattern, with a maximum gain of approximately 0 dB at 0° and 180°. The pattern features two distinct lobes, one at 0° and the other at 180°, with nulls at 90° and 270°. The antenna radiation patterns had a half-power beamwidth (HPBW) of 82.22° in the H-plane. It has an FBR of 20–25 dB. This implies that the antenna radiated more energy in the forward direction than in the backward.

3.2.2. Radiation Patterns at 4.24 GHz

E-Plane Pattern: The radiation pattern is nearly omnidirectional, with a slight variation in magnitude across different angles. The E-plane pattern at 4.24 GHz [Figure 9(c)] shows a similar omnidirectional radiation pattern to that at 3.52 GHz, with a maximum gain of 6–8 dB at 0° and 180°. However, there are nulls in the radiation pattern at around 90° and 270°, indicating that the antenna has reduced radiation in these directions. The antenna radiation patterns have an HPBW of 185.39° in the E-plane. It has an FBR of 10 dB to 12 dB.

H-Plane Pattern: The H-plane pattern at 4.24 GHz [Figure 9(d)] displays a more complex radiation pattern than that at 3.52 GHz. The radiation pattern was nearly omnidirectional, with slight variations in the magnitude at different angles. The pattern features multiple lobes and nulls, with a maximum gain of around -5 dB at 0°, and the antenna radiation patterns have HPBW 82.194° in H-plane. It also has an FBR of 10–12 dB.

3.2.3. Co-Polarization and Cross-Polarization Radiation Patterns

Co-polarization represents the signal power in the desired direction (used during transmission). The co-polarization (Co-Pol) and cross-polarization (X-Pol) knowledge is important for the knowledge of signal quality receptions and to know the isolation behaviour of the antenna in its transmission and reception modes. The E-plane and H-plane Co-Pol and X-Pol radiation patterns are shown in Figures 10(a)–(d) at two resonating frequencies 3.52 GHz and 4.24 GHz of the corner-truncated antenna. In general, the cross-polarization level is -20 dB–-30 dB lower than the co-polarization peak at boresight. These values of X-pol are necessary for the isolation of signal transmission and receptions without any interferences, and it also guarantees high signal quality reception, i.e., excellent signal

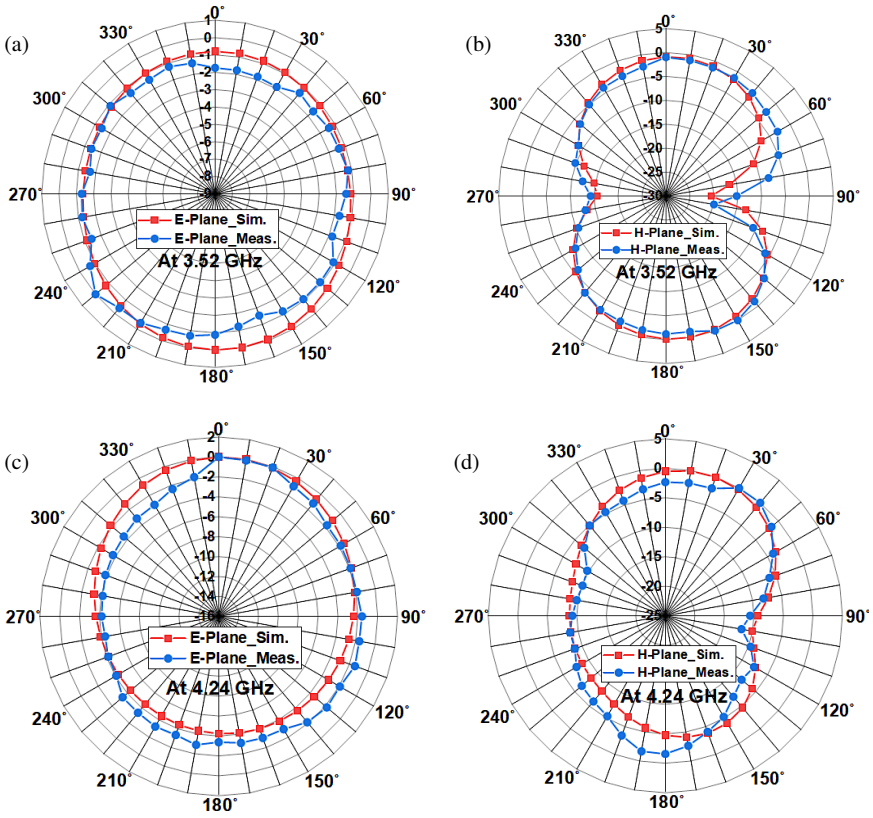

FIGURE 9. Radiation patterns plot (a) E-plane at 3.52 GHz, (b) H-plane at 3.52 GHz, (c) E-plane at 4.24 GHz, and (d) H-plane at 4.24 GHz.

to noise ratio (SNR). The four figures show the adequate lower values of the cross polarization concerning the co-polarization. E-plane Co-pol and X-pol differences are higher, which represents high quality signals [Figure 10(a) and Figure 10(c)] while H-plane Co-pol and X-pol discriminations are low, which corresponds to higher interference, indicating that electromagnetic power is "leaking" into the wrong polarization.

3.3. Antenna Axial Ratio and Polarization

The axial ratio of the proposed corner-truncated 5G antenna is shown in Figure 11. This figure illustrates the comparison of the axial ratios of the rectangular patch antenna, linear-truncated rectangular patch antenna, and linear and circular corner-truncated proposed flag-shaped microstrip antennas. The three important zones of polarization concerning the polarization types are marked in the figure with their axial ratio values. The rectangular patch antenna without corner truncation has linear polarization with axial ratio values exceeding 40 dB. When linear corners are truncated from the rectangular patch, the axial ratio value degrades in the entire wideband range of the antenna except for 4.40–4.70 GHz. In this range, the polarization nearly switched from the elliptical zone to the linear zone. Furthermore, circular corner truncation along with linear corner truncation decreases the value of the axial ratio towards the circular polarization zone, but its values still reside fully in the elliptical zone between 3 and 40 dB.

Polarization Purity: Cutting the corner of the radiating patch is a well-known method for creating circular polarization in patch antennas. The circular cuts ($a_1 = 3.0$ mm and $a_2 = 7.0$ mm) act as perturbations. These cuts vary the effective path length of the currents flowing diagonally. This truncation switches the linear polarization to circular polarization by reducing the axial ratio value close to 3 dB. With strip line feeding and corner truncation, it is difficult to realize polarization purity as required in a wideband response. The corners of the rectangular patch are truncated in a controlled manner to achieve stable polarization. In the proposed patch antenna, linear corner-truncation is very minor with 3.0 mm radius, while the circular-corner truncation is major with 7 mm radius. Therefore, the linear truncation switches the linear polarization to elliptical polarization, and circular corner truncation makes its axial ratio stable at 18 dB to 24 dB, resulting in stable elliptical polarization (part of linear polarization). Therefore, it is concluded that the corner truncation changes the antenna polarization from linear to elliptical polarization. The corner truncation with unequal dimensions on opposite corners causes orthogonal modes to be excited as discussed in Section 2.2.1, which turns the polarization of the antenna.

3.4. Antenna Gain and Antenna Efficiency

The simulated and measured gains and radiation efficiencies of the proposed antenna are shown in Figures 12(a)–(b). Good agreement was observed between the simulated and measured gains and radiation efficiencies. The peak simulated and measured gains at the two resonating frequencies were 3.93 and 4.25 dBi, respectively. The antenna's parasitic loading with

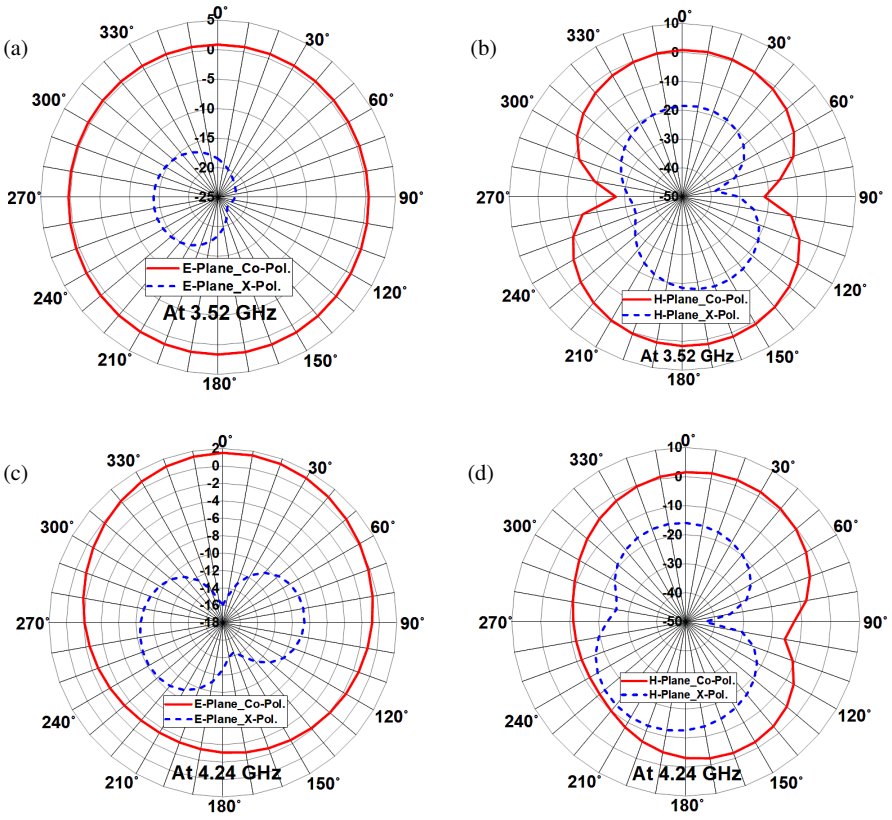

FIGURE 10. Co-polarization (co-pol.) and cross-polarization (X-Pol.) Radiation patterns plots (a) E-plane at 3.52 GHz, (b) H-plane at 3.52 GHz, (c) E-plane at 4.24 GHz, and (d) H-plane at 4.24 GHz.

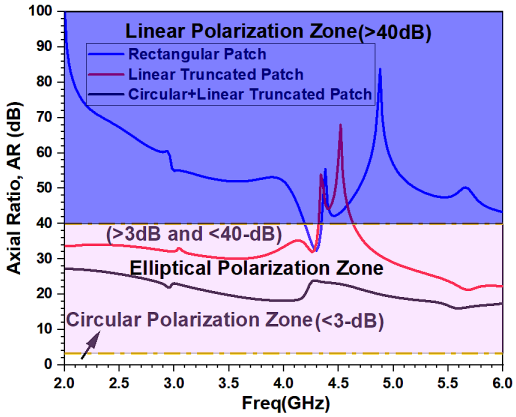

FIGURE 11. Antenna axial ratio.

a ground SRR causes gain values to decline between 4.0 and 4.40 GHz. The antenna achieves a radiation efficiency above 90% in the wide bandwidth of 2.82–5.21 GHz.

3.5. Surface Current Distribution

Figures 13(a)–(h) demonstrate the proposed antenna's surface current patterns at two resonant frequencies. The current density distribution magnitudes at lower (3.52 GHz) and upper (4.24 GHz) resonant frequencies are shown in Figures 13(a)–(d) and Figures 13(e)–(h), respectively. The surface current on a conventional rectangular patch is very small in magnitude, as shown in Figure 13(a). In Figure 13(b), two opposite corners of the rectangular patch are shortened to reduce charge accumulation across the corner bends and increase the current at the lowest resonant frequency, 3.52 GHz. The rectangular patch's two remaining corners are circularly truncated. Figures 13(c)–(d) show how this action changes the current distribution and reduces charge accumulations at the corners. With the same design and geometrical parameter settings as Figures 13(e)–(h), current distribution magnitudes are examined at 4.24 GHz, the higher resonant frequency. The current density magnitude varies significantly across the different plots, indicating changes in the antenna's operating conditions or design parameters. It is concluded that the antenna's performance is sensitive to the frequency of operation, with different current distributions observed at 4.24 GHz. These different current distributions are obvious because of the loading of the SRR. The concentration of current at specific points, such as the feed point and edges, indicates areas of high electromagnetic activity. In Figure 13(e), the current is mostly concentrated at the feed point and the lower parts of the antenna. In Figure 13(f), the current density magnitude is lower than Figure 13(e), with a maximum value of about 74.7814 A/m. The distribution is similar, with the current concentrated at the feed point and lower parts of the antenna. Figure 13(g) exhibits a significantly higher current density magnitude, with a maximum magnitude of 135.7538 A/m. The current is more evenly distributed across the antenna, with higher concentrations at the edges and corners. The current density magnitude in Fig-

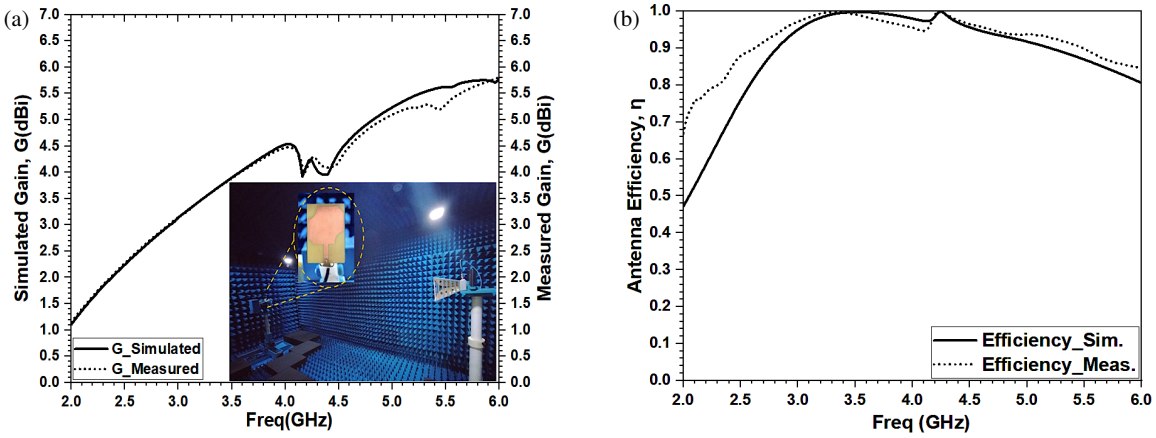

FIGURE 12. Simulated and measured (a) antenna gain, and (b) antenna efficiency.

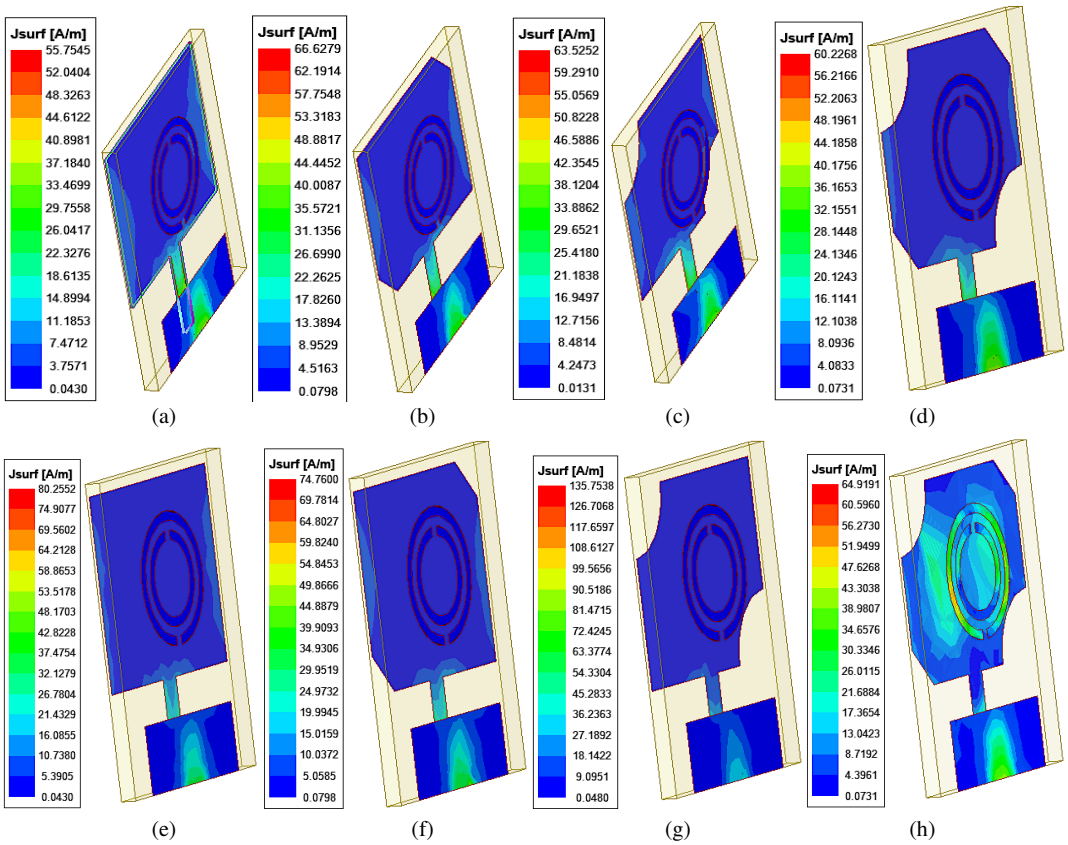

FIGURE 13. Surface current distributions antenna.

ure 13(h) is lower than that in Figure 13(g), with a maximum value of about 64.9191 A/m. The distribution is more uniform, with the current concentrated around the SRR and the feed point.

The truncation of opposite corners in the patch conjunctions with the monopole ground (reduced length and compressed width) results in the alteration of current distribution as shown in Figure 13, and this alteration of current distribution results in resonant and nearly orthogonal TM_{01} and TM_{10} modes generation in designs D2 and D3 which resonate near 2.55 GHz and 3.36 GHz. With designs D3 and D4, the current distribution alteration results in hybrid mode generation TM_{11}.

Figure 13 depicts a surface current distribution analysis that verifies the proposed antenna's dual-band technology. By comparing the distributions at 3.52 GHz and 4.24 GHz, the following observations support the resonance behavior: First Resonance (3.52 GHz): Figures 13(a)–(d) show that the surface current is primarily concentrated near the outside borders of the primary radiating patch and feed line. It means that the lower frequency band is mostly determined by the patch's overall effective electrical length. The relatively modest current intensity around the inner ring structures indicates that they are not the principal contributors to this resonance mode. Second Resonance (4.24 GHz): As the frequency rises to 4.24 GHz (Fig-

TABLE 7. Comparison with existing literature antennas.

Ref.	Antenna Shape and Feed Type	−10 dB BW (GHz)	f_r (GHz)	G (dBi)	Antenna Size (mm^3)	Size Min. (%)	Gnd.	Parasitic Loading	Application Covered
[2]	Spearhead antenna, wideband (WB), Transformer feed	FBW: 15.58% (3.28–3.83)	3.53	2.92	$13 \times 26 \times 1.6$ $(0.152\lambda_0 \times 0.303\lambda_0 \times 0.0186\lambda_0)$	85.33	Monopole	No parasitic loading	Wi-MAX, n78, 5G
[3]	Truncated corner monopole, edge-feed	FBW: 20.7% (3.285–3.87)	3.54	3.38	$12 \times 24 \times 1.6$ $(0.14\lambda_0 \times 0.28\lambda_0 \times 0.0186\lambda_0)$	86.74	Monopole	With rectangular stub	Wi-MAX, n78, 5G
[4]	Circular-truncated table lamp-shaped antenna, wideband (WB), Transformer feed	FBW: 16.57% (3.22–3.80)	3.50	2.88	$13 \times 26 \times 1.6$ $(0.152\lambda_0 \times 0.303\lambda_0 \times 0.0186\lambda_0)$	85.33	Monopole	No parasitic loading	Wi-MAX, n78, 5G
[6]	Rectangular patch with mutually coupled, edge feed	FBW: 55.14% (3.13–5.06)	3.50	5.14	$35.686 \times 31.688 \times 1.6$ $(0.416\lambda_0 \times 0.423\lambda_0 \times 0.0186\lambda_0)$	12.676	Monopole	With U-stub and SRR	Wi-MAX, n77, n78, n79, 5G
[9]	Slotted-circular patch, edge feed	FBW: 66% (3.04–5.35)	3.50	4.5	$35 \times 25 \times 1.6$ $(0.408\lambda_0 \times 0.291\lambda_0 \times 0.0186\lambda_0)$	0	Monopole	With stub	Wi-MAX, n77, n78, n79, 5G
[13]	Circular truncated four-corners, double slotted, edge feed	FBW: 30.5% (3.1–4.2), 19.6% (4.9–5.9), and 17% (6.4–7.6)	3.6, 5.1, 7.2	4.15	$28 \times 26 \times 1.6$ $(0.289\lambda_0 \times 0.268\lambda_0 \times 0.0165\lambda_0)$	0	Monopole, compressed ground	No parasitic loading	n77, n78, WLAN, Wi-Fi 5, WiFi 6E
[14]	Linear truncated two-corners, elliptical multi-orbital slotted, edge feed	FBW: 40.8% (5.5–6.725)	6.2	3.5	$20 \times 15 \times 1.6$ (PDMS) $(0.328\lambda_0 \times 0.387\lambda_0 \times 0.0187\lambda_0)$	0	Complete ground	No parasitic loading	Sub-6 GHz, 5.8 GHz high-speed wireless communication, HiperLAN WiFi 6E
[16]	Monopole backed by AMC reflector, circularly polarized, Wideband, CPW feed	FBW: 63.22% (2.91–5.6)	3.5	2.8, 3.6	$30 \times 20 \times 1.6$ $(0.3\lambda_0 \times 0.233\lambda_0 \times 0.0187\lambda_0)$	0	Monopole	No parasitic loading	Sub-6 GHz, n78, n77, n79
[17]	Side-edge dual-band antenna. Coaxial feed	FBW: 3.69% (5.32–5.52) 3.36% (6.15–6.36)	3.5	2.0, 6.0	$148 \times 73 \times 1.6$ $(1.726\lambda_0 \times 0.85\lambda_0 \times 0.0187\lambda_0)$	0	Monopole	No parasitic loading	5G and Wi-Fi 6
[18]	An antenna consists of a full circle, a semicircle, and a meander line	FBW: 55.8% (3.05–5.39) 39.9% (5.84–8.19)	5.8	2.28, 4.26	$40 \times 15 \times 1.6$ $(0.773\lambda_0 \times 0.29\lambda_0 \times 0.0309\lambda_0)$	0	Monopole	No parasitic loading	IoT and 5G-WiFi
[27]	Frequency reconfigurable microstrip slot antenna consists of a fork-shaped patch, also two triangular-shaped strips, edge feed	FBW: 182.75% (3–13.6) UWB	5.8	Not given	$20 \times 20 \times 0.8$ $(0.386\lambda_0 \times 0.386\lambda_0 \times 0.015\lambda_0)$	0	And one L-shaped defected ground structure	No parasitic loading	WiMAX, WLAN
Proposed work	Truncated corner Flag-shaped monopole, edge-feed	FBW: 68.28% (2.82–5.21)	3.52, 4.24	3.93, 4.25	$28 \times 33 \times 1.6$ $(0.328\lambda_0 \times 0.387\lambda_0 \times 0.0187\lambda_0)$	30.55	Compressed Monopole, SRR used	With SRR	Wi-MAX, n77, n78, n79, 5G

* Gnd.: Ground; Min.: Miniaturization; G: Peak Gain; f_r: resonating frequency.

ures 13(e)–(h)), a considerable shift in current density occurs. The current gets extremely concentrated around the parasitic elements' edges and etched concentric ring slots. Figure 13(h) shows that the secondary band is created by the disruption of the surface current path caused by these specific geometric features. Ground Plane Interaction: The current on the ground plane is rather steady but shows localized intensification around the feed gap at both frequencies, ensuring good impedance matching for both bands.

Additionally, it is very clear from Figure 13(d) that the first resonance at 3.52 GHz is because the patch length has the highest current density, and the feed and rest part of the patch have the lowest current density magnitude. Additionally, when SRR is added, the largest magnitude is concentrated along the largest patch section, and the current density magnitude spread across the length and width of the patch is lessened. This displays the proposed antenna's dual-resonating behavior, as seen in Figure 13(h).

3.6. Similar Antennas' Performance Comparisons

Table 7 compares the antenna performance parameters of the proposed design with those of previously published works with approximately the same design frequency of 3.5 GHz. The proposed design is simple, small, and easy to build on a 1.6-mm double-sided FR4 substrate. Figure 14 shows how the varied literature affects the antenna miniaturization gains and fractional bandwidth (FBW). Unlike other antennas, the proposed antenna's miniaturization retains a gain of 5 dBi and FBW of 70%. Research shows that antenna size miniaturization affects fractional bandwidth and gains, while maximum gain and FBW are reached with minimum miniaturization, 12.676%. The figure and table show that the maximum miniaturized antenna has a lower gain and FBW. The hybrid corner-truncated parasitic-loaded antenna has a wide bandwidth and gain with modest miniaturization and is loaded with only one SRR and no slots in its patch, making it simpler to structure. The future antenna gain can be increased by transforming it into a MIMO structure, array layout, frequency-selective surfaces, layered patches in a multilayer antenna, etc. Most size miniaturization results in a decrease in gain and wide bandwidths. The regular shape antenna, of course, achieved a wide bandwidth higher than 100% while its gain value becomes degraded. With the corner truncated, shaped patch, the authors tried to achieve a wide bandwidth with higher gain. The hybrid combination of linear and circular corner truncations results in a novel antenna design with a compact size, achieving higher gain along with sufficient bandwidth. The wider bandwidth ($> 100\%$) leads to covering many applications, and there are higher chances of interferences in in-band applications [23, 24]. This application's interference issues are also eliminated by this antenna with FBW 70%. The rectangular SRR designed in [25, 26], intended to estimate the permittivity of liquids and milk samples, while in the proposed antenna, a circular SRR was used along with the patch. The intention of the insertion of SRR was to achieve the second resonating frequency and reflection coefficient perturbation near 4.0 GHz.

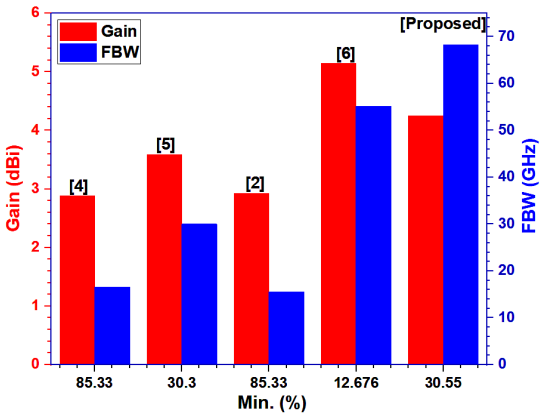

FIGURE 14. Antenna miniaturization effect on gain and FBW.

4. CONCLUSIONS

A hybrid (linear plus circular) corner-truncated antenna with a compact ground and parasitically SRR-loaded antenna was successfully modelled and investigated. The wideband (2.82–5.21 GHz) antenna achieves gains of 3.93 and 4.25 dBi at dual resonating frequencies within the band. The simulated and measured results are in agreement, indicating a well-modelled and fabricated antenna. Truncating the corners eliminated the charge accumulation around the rectangular bends of the patch. The cross-polarization radiation pattern is well below the co-polarization radiation patterns in E-plane and H-planes at two resonating frequencies, which confirms adequate signal transmission and reception with high quality and low signal interference. The antenna was miniaturized by 30.55% compared to a conventional rectangular patch antenna operating at the same frequency, which minimized the dielectric losses. The ohmic losses within the patch are reduced because of the lower requirement of copper in the patch. Therefore, the antenna achieves excellent stable efficiency of over 90% and elliptical polarization with a stable axial ratio between 15 and 20 dB within a wide bandwidth. Therefore, the wideband antenna is excellent for n77, n78, n79, n48, WiFi-5 (802.11ac), WiFi-6 (802.11ax), S-band, and C-band satellite, wireless, and radar applications. The gain of the proposed antenna is lower than that of a multiple-input multiple-output (MIMO) antenna array using a frequency-selective surface (FSS). Therefore, the proposed antenna can be explored as a MIMO and FSS structure to obtain sufficient gain values.

ACKNOWLEDGEMENT

The funding for this research was provided by the Ministry of Higher Education (MOHE) under the Fundamental Research Grant Scheme (FRGS), Grant No. FRGS/1/2025/TK07/UTEM/02/3, through Universiti Teknikal Malaysia Melaka. The authors would also like to extend their appreciation to Asia Pacific University (APU) for supporting this project.

REFERENCES

[1] Sharma, S., A. Kumar, R. Kumar, N. K. Saluja, Z. Zakaria, and A. J. A. Al-Gburi, "Miniaturized ultrawideband circularly polarized antenna with enhanced axial ratio bandwidth for C-band automotive and satellite applications," *Progress In Electromagnetics Research C*, Vol. 161, 159–168, 2025.

[2] Varshney, A., V. Sharma, T. M. Neebha, and R. Kumar, *A Compact Low-cost Impedance Transformer-fed Wideband Monopole Antenna for Wi-MAX N78-band and Wireless Applications*, 1st ed., 315–328, CRC Press, 2022.

[3] Varshney, A., V. Sharma, and A. K. Sharma, "RLC-equivalent circuit based stub loaded 2 × 2 MIMO antenna for wireless ap-

plications," *Microwave Review*, Vol. 29, No. 1, 44–54, 2023.

[4] Varshney, A., V. Sharma, T. M. Neebha, and N. P. Kumari, "Table lamp inspired miniaturized fractal antenna for 5G enabled green communications in smart cities," in *5G Green Communication Networks for Smart Cities*, 149–165, Apple Academic Press, 2025.

[5] Al-Gburi, A. J. A., "Do we really need frequency-selective surface and metasurface reflectors for antenna gain enhancement, or are metallic reflectors enough?" *International Journal of Antennas and Propagation*, Vol. 2026, No. 1, 2141943, 2026.

[6] Chidurala, S. and P. R. Amara, "Development and performance study of mutually coupled parasitically loaded 5G antenna for sub-6 GHz applications," *Sensing and Imaging*, Vol. 25, No. 1, 1–28, 2024.

[7] Al-Gburi, A. J. A., I. Ibrahim, Z. Zakaria, and A. D. Khaleel, "Bandwidth and gain enhancement of ultra-wideband monopole antenna using MEBG structure," *Journal of Engineering and Applied Sciences*, Vol. 14, No. 10, 3390–3393, 2019.

[8] Singh, S., V. Sharma, N. Sharma, and A. Varshney, "Lotus-shaped triple-tuned antenna with SRR quadruplets for SDARS and weather RADAR," *Microwave Review*, Vol. 30, No. 2, 23–35, 2024.

[9] Chidurala, S. and P. R. Amara, "Return loss and bandwidth improvement of circular ring antenna for 5G sub-6 GHz N77, N8 and, N79 band applications," in *2024 15th International Conference on Computing Communication and Networking Technologies (ICCCNT)*, 1–4, Kamand, India, 2024.

[10] Chidurala, S. and P. R. Amara, "Dual polarized firelight-shaped 4 port MIMO antenna using connected defected ground for 5G sub-6 GHz applications," *Physica Scripta*, Vol. 100, No. 6, 065534, 2025.

[11] Varshney, A., V. Sharma, T. M. Neebha, and N. P. Kumari, "Notch-band eliminator wideband CSRR loaded monopole fractal antenna for ISM and PCS communications," *World Journal of Engineering*, Vol. 21, No. 4, 821–834, 2024.

[12] Mathew, S., R. Anitha, U. Deepak, C. K. Aanandan, P. Mohanan, and K. Vasudevan, "A compact tri-band dual-polarized corner-truncated sectoral patch antenna," *IEEE Transactions on Antennas and Propagation*, Vol. 63, No. 12, 5842–5845, 2015.

[13] Bhattacharyya, S., A. Bhowmik, and K. Chatterjee, "Compact multiband MIMO antenna for sub-6 GHz 5G applications," *Wireless Personal Communications*, Vol. 140, No. 1, 713–737, 2025.

[14] Singh, T., P. Sharma, S. Tripathi, and V. S. Tripathi, "Elliptical multi orbital truncated flexible patch antenna using PDMS substrate for sub 6 GHz applications," *Defence Science Journal*, Vol. 74, No. 4, 546–551, 2024.

[15] Banerjee, U., A. Karmakar, and A. Saha, "A review on circularly polarized antennas, trends and advances," *International Journal of Microwave and Wireless Technologies*, Vol. 12, No. 9, 922–943, 2020.

[16] Askari, H., N. Hussain, D. Choi, M. A. Sufian, A. Abbas, and K. Nam, "An AMC-based circularly polarized antenna for 5G sub-6 GHz communications," *Computers, Materials, & Continua*, Vol. 69, No. 3, 2997–3013, 2021.

[17] Alsukour, M. and Y. S. Faouri, "Side-edge dual-band antenna for 5G and Wi-Fi 6 applications," in *2022 Microwave Mediterranean Symposium (MMS)*, 1–4, Pizzo Calabro, Italy, 2022.

[18] Al Ka'bi, A., "Proposed antenna design for IoT and 5G-WiFi applications," in *2022 IEEE World AI IoT Congress (AIIoT)*, 786–790, Seattle, WA, USA, 2022.

[19] Ouyang, Y. and W. J. Chappell, "High frequency properties of electro-textiles for wearable antenna applications," *IEEE Transactions on Antennas and Propagation*, Vol. 56, No. 2, 381–389, 2008.

[20] Balanis, C. A., *Antenna Theory: Analysis and Design*, 3rd ed., John Wiley & Sons, New Jersey, 2016.

[21] Purohit, S. and F. Raval, "Wearable-textile patch antenna using jeans as substrate at 2.45 GHz," *International Journal of Engineering Research & Technology (IJERT)*, Vol. 3, No. 5, 2456–2460, 2014.

[22] Yang, L., L. J. Martin, D. Staiculescu, C. P. Wong, and M. M. Tentzeris, "Conformal magnetic composite RFID for wearable RF and bio-monitoring applications," *IEEE Transactions on Microwave Theory and Techniques*, Vol. 56, No. 12, 3223–3230, 2008.

[23] Varshney, A., S. Kumar, R. Dwivedi, and N. Nurhayati, "Circular layout hybrid patch CSRR loaded antenna for sub-6 GHz n77, n78, n79 band applications with applications-interference eliminations," *E3S Web of Conferences*, Vol. 645, 04005, 2025.

[24] Varshney, A., S. Kumar, D. N. Gençoğlan, S. Tiwari, S. Ara, I. Elfergani, C. Zebiri, and J. Rodriguez, "Compact metasurface antenna for sub-6 GHz applications with isolated n77/n78 bands using CSRR," *Physica Scripta*, Vol. 100, No. 1, 015508, 2025.

[25] Kiani, S., P. Rezaei, and M. Navaei, "Dual-sensing and dual-frequency microwave SRR sensor for liquid samples permittivity detection," *Measurement*, Vol. 160, 107805, 2020.

[26] Navaei, M., P. Rezaei, and S. Kiani, "Microwave split ring resonator sensor for determination of the fluids permittivity with measurement of human milk samples," *Radio Science*, Vol. 57, No. 7, 1–11, 2022.

[27] Kakhki, M. B. and P. Rezaei, "Reconfigurable microstrip slot antenna with DGS for UWB applications," *International Journal of Microwave and Wireless Technologies*, Vol. 9, No. 7, 1517–1522, 2017.